AMERICAN SOCIETY FOR MICROBIOLOGY | Molecular and Cellular Biology®

RESEARCH ARTICLE

Ras Suppresses TXNIP Expression by Restricting Ribosome Translocation

Zhizhou Ye,[a] Donald E. Ayer[a]

[a]Department of Oncological Sciences, Huntsman Cancer Institute, University of Utah, Salt Lake City, Utah, USA

ABSTRACT Oncogenic Ras upregulates aerobic glycolysis to meet the bioenergetic and biosynthetic demands of rapidly growing cells. In contrast, thioredoxin-interacting protein (TXNIP) is a potent inhibitor of glucose uptake and is frequently downregulated in human cancers. Our laboratory previously discovered that Ras activation suppresses TXNIP transcription and translation. In this study, we developed a system to study how Ras affects TXNIP translation in the absence of transcriptional effects. We show that whereas Ras drives a global increase in protein translation, it suppresses TXNIP protein synthesis by reducing the rate at which ribosomes transit the coding region of TXNIP mRNA. To investigate the underlying mechanism(s), we randomized or optimized the codons in the TXNIP message without altering the TXNIP primary amino acid sequence. Translation from these mRNA variants was still repressed by Ras, implying that mRNA secondary structure, microRNAs (miRNAs), RNA binding proteins, or codon usage does not contribute to the blockade of TXNIP synthesis. Rather, we show that the N terminus of the growing TXNIP polypeptide is the target for Ras-dependent translational repression. Our work demonstrates how Ras suppresses TXNIP translation elongation in the face of a global upregulation of protein synthesis and provides new insight into Ras-dependent metabolic reprogramming.

KEYWORDS oncogenic Ras, TXNIP, translation elongation, protein synthesis, metabolic reprogramming, Warburg effect, glucose, MondoA, metabolic regulation, translational control

Activating mutations in the small Ras GTPases (K-Ras, H-Ras, and N-Ras) are among the most common alterations in human cancer. The oncogenic mutations render the Ras proteins constitutively active, which drives uncontrolled proliferation through the activation of the downstream signaling pathways, such as the mitogen-activated protein kinase (MAPK) and phosphatidylinositol 3-kinase (PI3K) pathways (1, 2). Ras activation also rewires metabolism to accommodate the increased anabolic demands of rapidly growing and dividing cells. For example, Ras stimulates glucose uptake and aerobic glycolysis for ATP generation, diverts glycolytic intermediates into biosynthetic pathways, and upregulates glutaminolysis to fuel central carbon metabolism (3–5). The glycolytic switch conferred by Ras activation has been classically ascribed to its activation of c-Myc and hypoxia-inducible factor 1α (HIF-1α), which directly drive the expression of glucose transporters and glycolytic enzymes (6–8). More recent transcriptional analysis showed that oncogenic Ras activates the expression of genes involved in a spectrum of anabolic pathways, including the hexosamine-, ribose-, and pyrimidine-biosynthetic pathways (9). Each of these biosynthetic pathways is fueled by glucose-derived carbons. However, in the absence of glucose availability, flux through these biosynthetic pathways is limited. Thus, nutrient use must be coupled with nutrient availability to sustain the rapid growth and division of transformed cells.

Thioredoxin-interacting protein (TXNIP) is a critical negative regulator of cellular

Received 10 April 2018 **Returned for modification** 2 May 2018 **Accepted** 16 July 2018

Accepted manuscript posted online 23 July 2018

Citation Ye Z, Ayer DE. 2018. Ras suppresses TXNIP expression by restricting ribosome translocation. Mol Cell Biol 38:e00178-18. https://doi.org/10.1128/MCB.00178-18.

Address correspondence to Donald E. Ayer, don.ayer@hci.utah.edu.

glucose uptake. It inhibits glucose uptake by removing glucose transporters from the cell surface (10, 11). Consequently, TXNIP loss is sufficient to drive glucose uptake and aerobic glycolysis (12–15). Further, TXNIP can also promote oxidation of nonglucose fuels (16, 17). Therefore, low TXNIP levels support the use of glucose as a fuel, whereas high TXNIP levels support the use of nonglucose fuels. In addition to this function in fuel choice, TXNIP has a number of additional antiproliferative activities. For example, it can drive apoptosis by activating Ask1, and it can drive cell cycle arrest by stabilizing $p27^{kip1}$ (18, 19). Given these assorted functions, it is not surprising that TXNIP functions as a tumor suppressor and is downregulated in a variety of human cancers (20–22).

Transcription of the TXNIP gene is highly, if not entirely, dependent on the MondoA transcription factor (20, 23). MondoA is a member of the extended Myc network, and its activity is driven by high glucose levels (24). Thus, the MondoA-TXNIP axis constitutes a negative-feedback loop that regulates glucose homeostasis (15, 25, 26). Our previous work established that the MondoA-TXNIP axis is downregulated by PI3K, mTOR, or Myc activation, which contributes to their well-characterized activities in driving aerobic glycolysis (20, 27, 28). TXNIP is also subject to posttranslational regulation in response to signaling pathways. For example, under energy depletion, AMPK phosphorylates TXNIP, leading to its degradation and permitting increased glucose uptake to restore energy homeostasis (10). The general model that emerges from these studies is that progrowth signals downregulate TXNIP, which subsequently supports aerobic glycolysis and, presumably, anabolic reactions.

Our laboratory has previously shown that Ras activation downregulates TXNIP mRNA and protein expression (27). We propose that TXNIP repression provides an additional route to increase glucose uptake and utilization in response to Ras activation. In this study, we investigated how Ras inhibits TXNIP expression, with a focus on posttranscriptional regulation. We show that in spite of driving increased global translation, Ras suppresses translation elongation of TXNIP mRNA by targeting the N terminus of the nascent TXNIP polypeptide chain as it exits the ribosome exit tunnel.

RESULTS

Ras^{G12V} inhibits TXNIP expression. Our previous data suggest that acute Ras activation in immortalized human fibroblasts suppresses TXNIP transcription and translation (27). Consistent with Ras blocking TXNIP transcription, we observed a negative correlation between an H-Ras gene signature and TXNIP expression in breast cancer, lung adenocarcinoma, and pancreatic adenocarcinoma patient samples using publicly available data sets (Fig. 1A). Experimentally, expression of activated H-Ras (Ras^{G12V}) in murine embryonic fibroblasts (MEFs) completely abolished TXNIP mRNA and protein expression (Fig. 1B and C). The complete suppression of TXNIP transcription prevented us from investigating whether Ras^{G12V} regulates TXNIP posttranscriptionally.

To overcome this hurdle, we stably expressed the human TXNIP coding region in MondoA knockout (KO) MEFs under the control of a constitutive promoter (i.e., control cells) and examined the effects of Ras activation by expressing Ras^{G12V} (i.e., Ras^{G12V}-expressing cells). All subsequent experiments were conducted using these cells unless otherwise specified. MondoA KO MEFs lack endogenous TXNIP expression, enabling investigation of TXNIP expression from the exogenous TXNIP allele (Fig. 1D). In this experimental system, the level of ectopic TXNIP mRNA was higher in Ras^{G12V}-expressing cells than in control cells (Fig. 1E), yet TXNIP protein expression was dramatically repressed by Ras^{G12V} (Fig. 1F). This experiment suggests that Ras activation induces TXNIP protein degradation or suppresses TXNIP synthesis.

Ras^{G12V} inhibits TXNIP translation. We determined whether Ras^{G12V} increases the rate of TXNIP protein degradation using two methods. We first measured TXNIP protein degradation by blocking *de novo* protein synthesis with cycloheximide (CHX). We observed that the half-life of TXNIP protein was about 1 h in control cells and slightly shorter (about 40 min) in Ras^{G12V}-expressing cells, suggesting that Ras activation can increase TXNIP turnover (Fig. 2A and B). Consistent with this finding, the proteasome inhibitor MG132 also increased TXNIP protein levels in Ras^{G12V}-expressing cells, but the

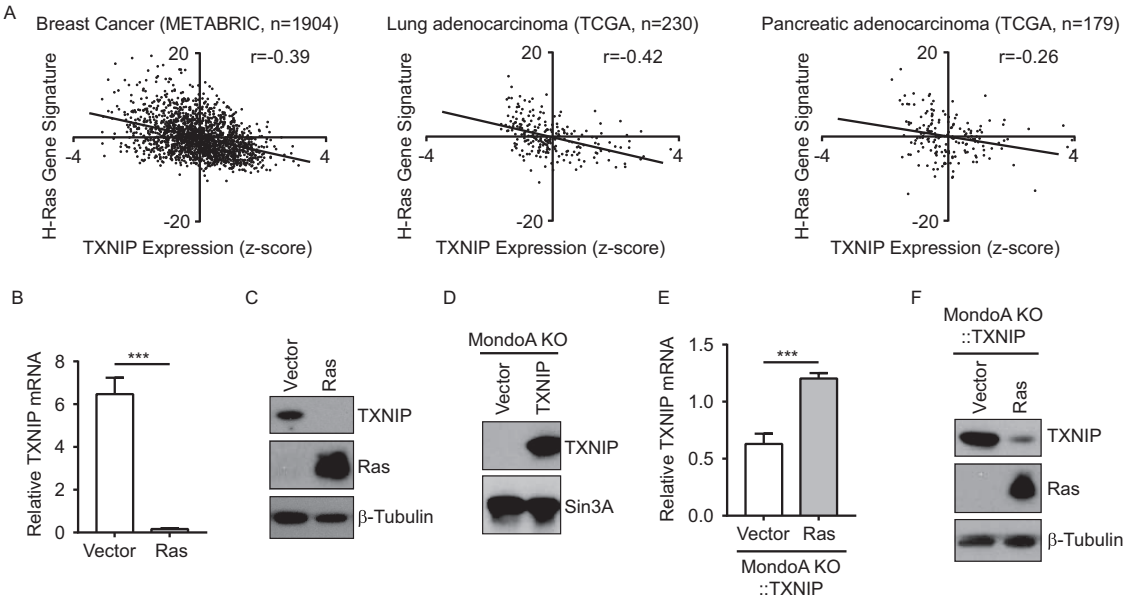

FIG 1 Ras^{G12V} inhibits TXNIP expression. (A) Scatter plots showing the relationship between the H-Ras gene signature and the TXNIP mRNA expression level. Each point represents a single tumor sample from the indicated cancer data set, with sample size indicated. The correlation coefficient, Pearson's *r*, is shown for each data set. (B and C) RT-qPCR (B) and Western blotting (C) were used to determine relative TXNIP mRNA levels (normalized to that of β-actin) and levels of the indicated proteins, respectively, in wild-type MEFs stably transduced with pBabePuro (Vector) or pBabePuro-H-Ras^{G12V} (Ras). (D) Western blotting was used to determine the levels of TXNIP and Sin3A proteins in MondoA KO MEFs stably transduced with pWzlBlast (Vector) or pWzlBlast-TXNIP CDS (TXNIP). (E and F) MondoA KO::TXNIP MEFs were stably transduced with pBabePuro (Vector) or pBabePuro-H-Ras^{G12V} (Ras), as indicated. RT-qPCR (E) and Western blotting (F) were used to determine relative TXNIP mRNA levels (normalized to that of β-actin) and the levels of the indicated proteins in each cell population. The experiments shown in panels B and E were repeated at least twice, and representative experiments are shown. Values are reported as means and SD. Statistical significance was determined using *t* tests. ***, $P < 0.001$.

increase was not to the levels observed in control cells (Fig. 2C), suggesting that increased degradation cannot fully account for lower TXNIP protein expression in Ras^{G12V}-expressing cells.

A number of previous publications have focused on TXNIP degradation (10, 29); therefore, we elected to investigate whether Ras^{G12V} affects the rate of TXNIP protein synthesis. Newly synthesized proteins were identified by labeling cells with a methionine analog (azidohomoalanine [AHA]). Following labeling, cell lysates were prepared, and proteins that incorporated the AHA label were biotinylated using click chemistry and then enriched on streptavidin beads. Cells were also treated with MG132 to eliminate degradation, allowing us to examine the effects on TXNIP synthesis alone. As expected, Ras^{G12V}-expressing cells expressed less TXNIP than control cells at steady state. Importantly, Ras^{G12V}-expressing cells had significantly less newly synthesized TXNIP during 1-h or 3-h labeling periods (Fig. 2D). These data suggest that Ras^{G12V}, in addition to triggering TXNIP degradation, also suppresses TXNIP protein synthesis.

To examine inhibition of TXNIP synthesis by activated Ras in more detail, we designed a luciferase reporter assay. In this assay, the TXNIP coding region (TXNIP CDS) was fused upstream of and in frame with the open reading frame (ORF) encoding destabilized luciferase (dsLuc) (Fig. 2E). Therefore, the translation of dsLuc, and the subsequent luciferase activity, was controlled by translation through the TXNIP CDS. To minimize transcriptional effects, expression of dsLuc or TXNIP-dsLuc was driven from a constitutive promoter. dsLuc is a fusion of the luciferase open reading frame with CL1 and hPEST destabilization sequences, which confer a half-life of 0.4 h. In the presence of CHX, dsLuc activity decreased at similar rates in control and Ras^{G12V}-expressing cells, with a half-life very close to the reported value. In addition, the activity of TXNIP-dsLuc also decreased at similar rates in both cell types, suggesting the degradation of TXNIP-dsLuc is dominated by the turnover of dsLuc and is not affected by Ras^{G12V} (Fig. 2F). TXNIP-dsLuc protein was intact, and its level correlated well with its activity

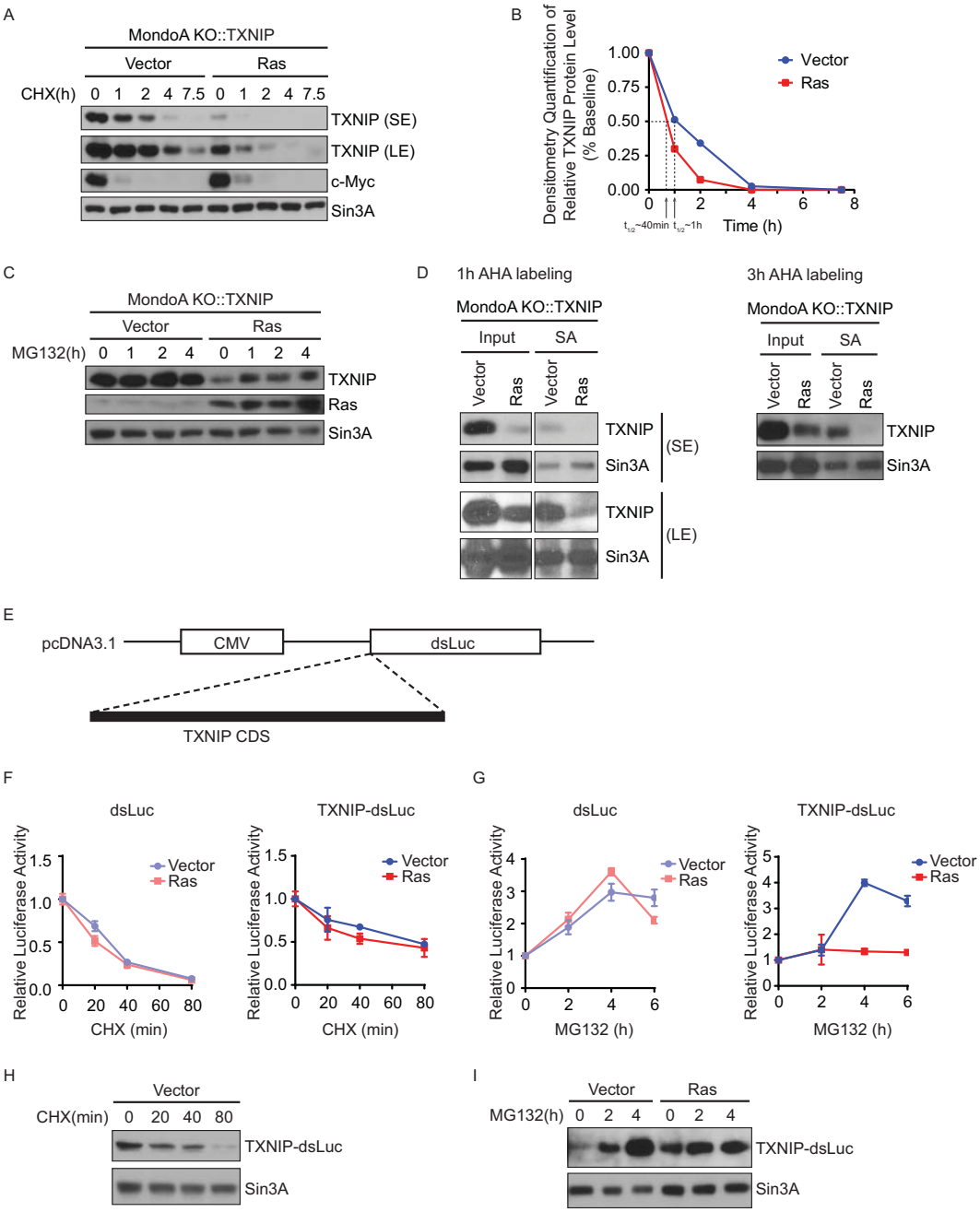

FIG 2 Ras^{G12V} inhibits TXNIP translation. (A) Western blotting was used to determine the levels of the indicated proteins in the listed cell lines following a time course of treatment with 40 μg/ml CHX. Short (SE) and long (LE) exposures allowed better visualization of the TXNIP signal. c-Myc and Sin3A served as controls for proteins that turn over rapidly or slowly. (B) TXNIP protein levels in panel A were quantified using densitometry. Signals from short exposures or long exposures were used for quantification of the control cells (Vector) or the Ras^{G12V}-expressing cells (Ras), respectively. The half-life ($t_{1/2}$) of TXNIP protein in each cell line was determined and is indicated in the plot. (C) Western blotting was used to determine the levels of the indicated proteins in the listed cell lines following a time course of treatment with 20 μM MG132. (D) Newly synthesized proteins were enriched by labeling cells with AHA for 1 h or 3 h, followed by biotinylation using click chemistry and affinity purification using streptavidin beads (SA). Western blotting was used to determine the levels of steady-state (Input) and newly synthesized (SA) TXNIP and Sin3A proteins in the indicated cell lines. (E) Diagram of the pcDNA3.1-TXNIP-dsLuc2CP construct, in which the human TXNIP CDS was cloned upstream of and in frame with the destabilized luciferase ORF (dsLuc). CMV, cytomegalovirus. (F and G) Luciferase reporters were transfected into MondoA KO::TXNIP::Vector (Vector) or Ras^{G12V} (Ras) MEFs. Relative luciferase activity, normalized to β-Gal activity, of TXNIP-dsLuc or dsLuc was determined following time courses of treatment with 40 μg/ml CHX (F) or 20 μM MG132 (G) in the indicated cell lines. The luciferase experiments were repeated at least twice, and representative experiments are shown. Values are reported as means and SD. (H and I) TXNIP-dsLuc was transfected into MondoA KO::TXNIP::Vector (Vector) or Ras^{G12V} (Ras) MEFs. Western blotting was used to determine the TXNIP-dsLuc levels following time courses of treatment with 40 μg/ml CHX (H) or 20 μM MG132 (I) in the indicated cell lines.

(Fig. 2H). Thus, this reporter system allowed us to investigate how Ras^{G12V} regulates TXNIP protein synthesis.

To focus only on TXNIP synthesis, we blocked proteasome activity with MG132. In the presence of MG132, Ras^{G12V} did not affect the accumulation of dsLuc activity. In contrast, the activity of TXNIP-dsLuc was significantly lower in Ras^{G12V}-expressing cells than in control cells (Fig. 2G). Consistent with these findings, TXNIP-dsLuc protein increased over the course of MG132 treatment in control cells, whereas it did not increase in Ras^{G12V}-expressing cells (Fig. 2I). Notably, the baseline level of TXNIP-dsLuc was higher in Ras^{G12V}-expressing cells than in control cells (Fig. 2I), likely because Ras^{G12V}-expressing cells have a higher transfection efficiency than control cells. Together, these experiments suggest that Ras^{G12V} suppresses TXNIP expression primarily by decreasing TXNIP synthesis, with an increase in TXNIP degradation as a secondary contributing factor. Furthermore, the TXNIP CDS is sufficient to confer Ras^{G12V}-dependent blockade of TXNIP synthesis, indicating that 5′ and 3′ untranslated regions of the TXNIP mRNA are not responsible for the Ras^{G12V} blockade.

Ras^{G12V} inhibits translation elongation of TXNIP mRNA. Growth factor signaling promotes global protein synthesis (30, 31). Therefore, it is paradoxical that Ras^{G12V} suppresses TXNIP synthesis. To explore this contradiction further, we first determined whether Ras^{G12V} enhances global protein synthesis in MEFs, using AHA labeling. As expected, global protein synthesis was increased after Ras activation (Fig. 3A). Thus, even though Ras activation increases global translation, it suppresses translation of the TXNIP mRNA.

Since the TXNIP CDS is sufficient for translational repression by Ras^{G12V} (Fig. 2D and G), we hypothesized that Ras^{G12V} restricts TXNIP synthesis by blocking translation elongation of the TXNIP message. To test this hypothesis, we used polysome profiling to determine how Ras^{G12V} affects the distribution of ribosomes on the TXNIP mRNA and other messages. To gauge the elongation rate, we used harringtonine, which inhibits translation by immobilizing initiating ribosomes at the start codon without affecting elongating ribosomes. Thus, the rate at which ribosomes are cleared from individual mRNAs in the presence of harringtonine can be used to estimate the elongation rate (32, 33). Cell lysates from control and Ras^{G12V}-expressing cells were subjected to velocity sedimentation in a sucrose gradient, and the gradient was subsequently fractionated. The bulk RNA content, which reflects rRNA-containing ribosomes in association with mRNA, was monitored by measuring the optical density at 254 nm (OD_{254}) across the gradient (Fig. 3B). RNA was purified from each fraction, and the levels of gene transcripts of interest were determined by reverse transcription-quantitative PCR (RT-qPCR). We examined the abundance of heavy-polysome-associated mRNAs (fractions F7 and F8) from control and Ras^{G12V}-expressing cells before and after harringtonine treatment (Fig. 3B). We next calculated the percent decrease in heavy-polysome-associated RNAs of interest caused by harringtonine treatment.

At the bulk RNA level (Fig. 3B), we observed that Ras^{G12V}-expressing cells had significantly more heavy-polysome-associated mRNA than control cells, confirming that Ras activation drives global translation. Moreover, the majority of heavy-polysome-associated mRNA diminished in the presence of harringtonine in both cell types, suggesting effective clearance of ribosomes from the majority of mRNA transcripts (Fig. 3B). Confirming the result with bulk RNA, 5srRNA, which is a component of the ribosome, was more abundant in heavy-polysome fractions from Ras^{G12V}-expressing cells than in those from control cells and was cleared from the heavy-polysome fractions following harringtonine treatment (Fig. 3C). Similarly, there was more heavy-polysome-associated TXNIP mRNA from Ras^{G12V}-expressing cells than from control cells. However, in response to harringtonine treatment, the amount of TXNIP mRNA associated with heavy polysomes decreased less in Ras^{G12V}-expressing cells (23% decrease) than in control cells (28% decrease), suggesting that active Ras lowers the rate at which ribosomes transit the TXNIP message (Fig. 3D). For comparison, we examined actin mRNA, a housekeeping gene expected to be translated efficiently. The

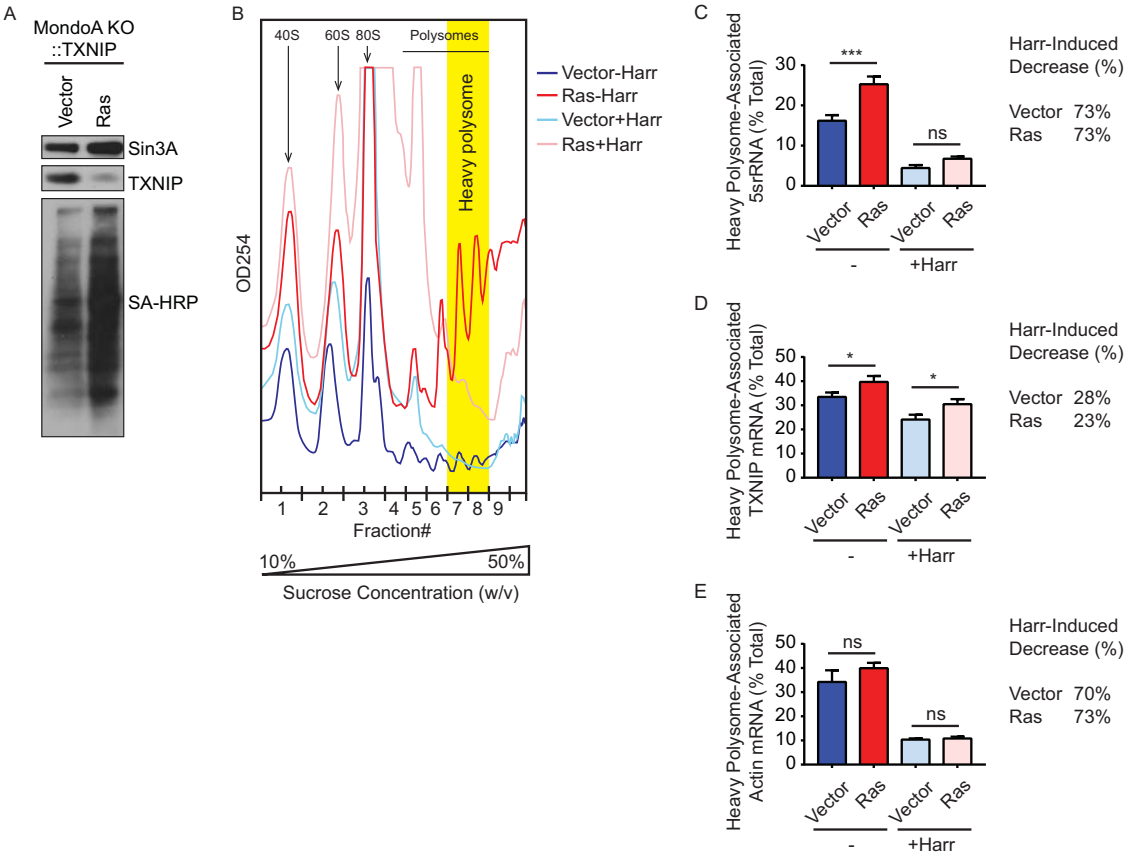

FIG 3 Ras^{G12V} inhibits translation elongation of TXNIP mRNA (A) Cells were labeled with AHA for 2 h. Click chemistry was used to biotinylate the labeled proteins. Western blotting was used to determine the levels of TXNIP and Sin3A proteins and newly synthesized proteins (SA-HRP) in the indicated cell lines. (B) Chromatograms showing the polysome profile of MondoA KO::TXNIP::Vector (Vector) or Ras^{G12V} (Ras) MEFs before (−Harr) and after (+Harr) harringtonine treatment. Fraction numbers are shown on the *x* axis, with heavy-polysome fractions shaded in yellow. (C to E) RT-qPCR was used to determine the amounts of 5srRNA (C), TXNIP mRNA (D), and actin mRNA (E) from heavy-polysome fractions of the listed cell population. The amount of heavy-polysome-associated RNA was normalized to that of total RNA. The percent decrease in heavy-polysome-associated RNA levels caused by harringtonine treatment was calculated for each cell line. Experiments were repeated twice, and a representative experiment is shown. Values are reported as means and SD. Statistical significance was determined using one-way ANOVA. *, $P < 0.05$; ***, $P < 0.001$; ns, $P \geq 0.05$.

amounts of heavy-polysome-associated actin mRNA were comparable and decreased similarly in both cell types after harringtonine treatment, suggesting that translation of actin mRNA is not affected by Ras^{G12V} (Fig. 3E). Together, these data support a model where ribosomes transit the TXNIP message relatively slowly and are slowed even further with Ras activation.

The translation elongation rate does not correlate with gene function. We wondered whether Ras's blockade of elongation is restricted to TXNIP or whether it suppresses translation more broadly. To investigate this question, we analyzed data from a ribosome profiling experiment designed to examine translation elongation in mouse embryonic stem cells (mESCs) (33). We generated an elongation profile for each gene transcript by calculating the change in the relative ribosome density across the CDS caused by harringtonine treatment. We next performed unsupervised clustering on the top 9,962 translationally active gene transcripts based on their elongation profiles. The 9,962 genes were segregated into 10 clusters (C1 to C10) with a wide dynamic range. For example, ribosomes on transcripts from C1, C3, C9, and C10 elongate extremely fast, whereas ribosomes on transcripts from C4, C6, and C8 elongate extremely slowly (Fig. 4A). An example of a "fast" gene is Hist1h2bc in C3, whereas an example of a "slow" gene is Epha2 in C8 (Fig. 4B and C). Consistent with our polysome profiling data, ribosomes run off the TXNIP message, found in C7, relatively

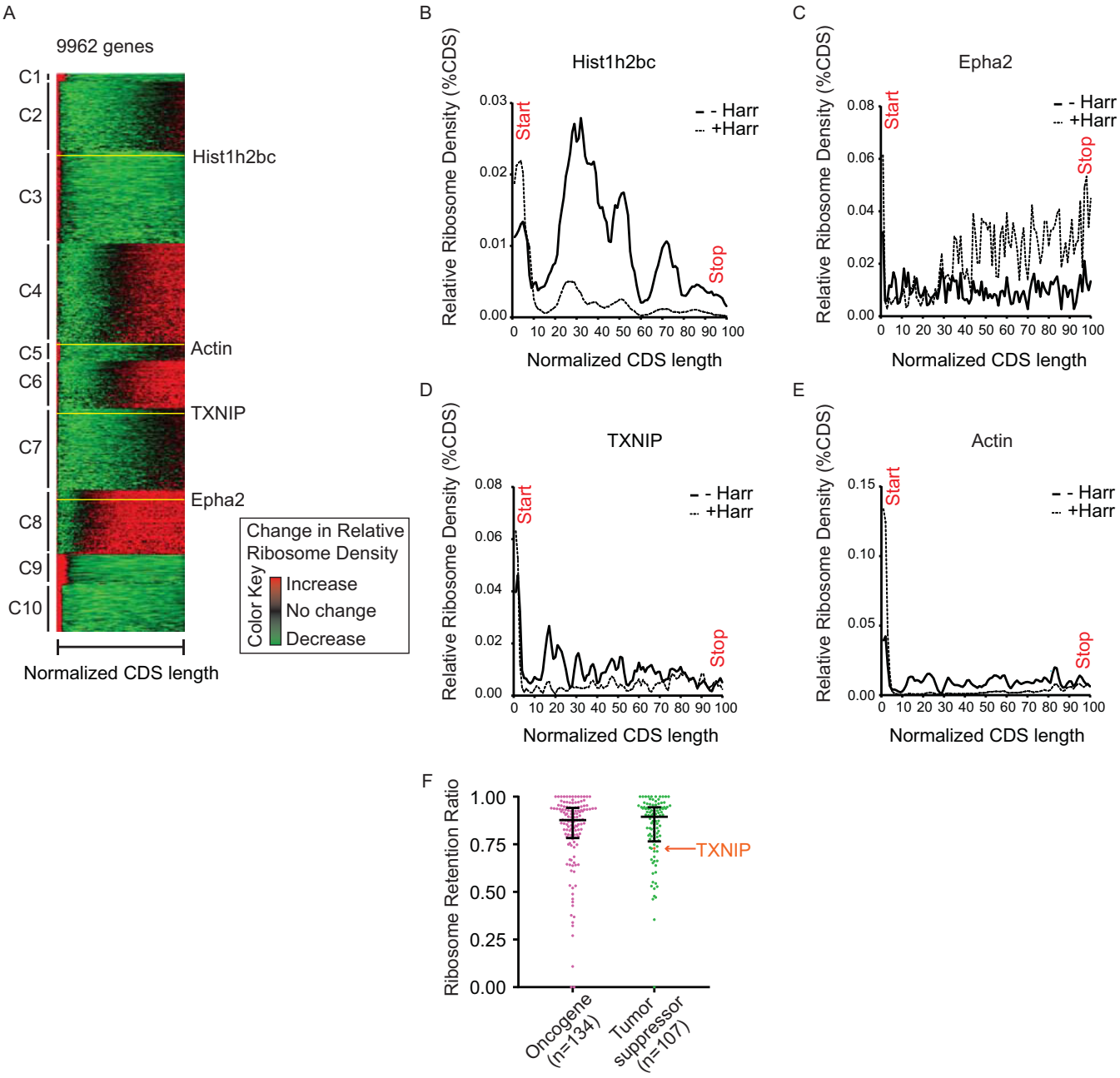

FIG 4 The translation elongation rate does not correlate with gene function. (A) Heat map showing unsupervised clustering on the top 9,962 translationally active gene transcripts in mESCs based on their elongation profiles, which were generated by calculating the change of relative ribosome density across the CDS of each transcript caused by 120 s of harringtonine treatment. Red and green indicate increased and decreased relative ribosome density after harringtonine treatment, respectively. The Hist1h2bc, Epha2, TXNIP, and actin transcripts are indicated by yellow lines. (B to E) Ribosome profiling data showing the relative ribosome density across the CDS of Hist1h2bc, Epha2, TXNIP, and actin transcripts in mESCs before (−Harr) and after (+Harr) 120 s of harringtonine treatment. (F) Grouped scatter plot showing the ribosome retention ratios of 134 oncogenes and 107 tumor suppressors, with median and interquartile range indicated on the plot.

slowly whereas they run off the actin message, found in C5, relatively quickly (Fig. 4D and E). We performed pathway analysis for the genes in C7 and found that the cluster was not enriched for growth suppressors. Therefore, messages with elongation dynamics similar to those of TXNIP do not generally encode growth suppressors. Further, this finding suggests that Ras suppression of translation elongation might be restricted to TXNIP mRNA.

Even though growth suppressors did not cluster with TXNIP, we wondered whether tumor suppressors and oncogenes have different elongation dynamics, allowing dif-

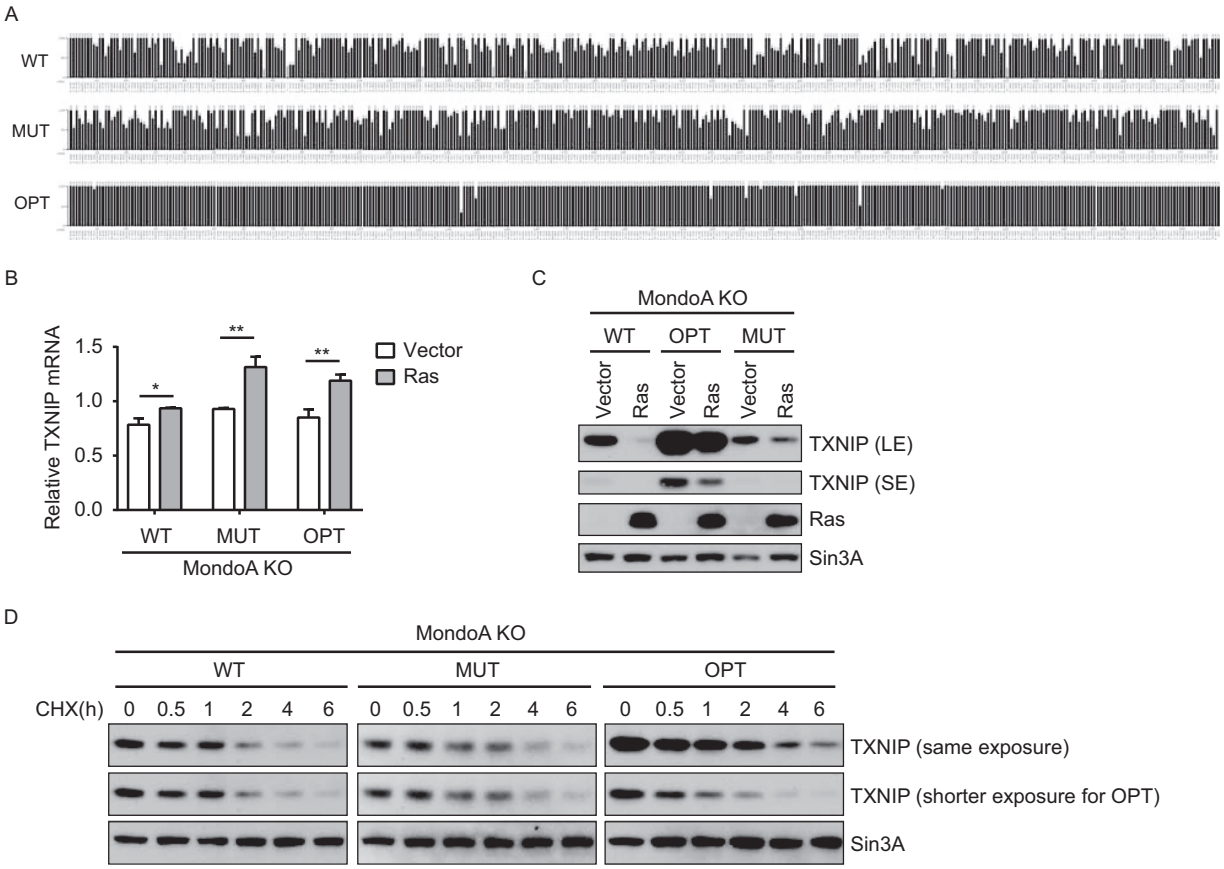

FIG 5 TXNIP mRNA primary sequence is not required for Ras^{G12V}-dependent translational repression. (A) Diagram showing the relative adaptiveness of each codon of TXNIP-WT, -MUT, and -OPT. (B and C) MondoA KO MEFs were stably transduced with TXNIP variants (WT, MUT, or OPT), each of which was further stably transduced with pBabePuro (Vector) or pBabePuro-H-Ras^{G12V} (Ras), as indicated. RT-qPCR (B) and Western blotting (C) were used to determine relative TXNIP mRNA levels (normalized to that of β-actin) and the levels of the indicated proteins in each cell population. Long (LE) and short (SE) exposures allowed better visualization of the TXNIP signal. (D) MondoA KO MEFs were stably transduced with TXNIP variants (WT, MUT, or OPT). Western blotting was used to determine the levels of the indicated proteins in each cell population following a time course of treatment with 40 μg/ml CHX. The same exposure is shown for comparison of expression levels of the three TXNIP variants; a shorter exposure is shown for TXNIP-OPT for comparison of degradation rates among different TXNIP variants. The values in panel B are reported as means and SD. Statistical significance was determined using a *t* test. *, $P < 0.05$; **, $P < 0.01$.

ferential translational regulation by Ras or other oncogenic lesions. By comparing the ribosome retention ratios of 134 oncogenes and 107 tumor suppressors, we observed that the two groups had similar elongation dynamics (Fig. 4F). Together, these results suggest that rapid elongation dynamics are not generally associated with messages encoding oncoproteins, nor are slow elongation dynamics associated with messages encoding tumor suppressors.

TXNIP mRNA primary sequence is not required for Ras^{G12V}-dependent translational repression. We next investigated whether the sequence of the TXNIP message contributed to the Ras^{G12V}-dependent blockade of translation elongation. First, we tested the contribution of the primary sequence of the TXNIP mRNA. We used gene synthesis to create a TXNIP mRNA with extensive silent mutations across the entire CDS, TXNIP-MUT. The TXNIP-MUT mRNA is comprised of codons with usage frequencies similar to those present in the wild-type TXNIP (TXNIP-WT) mRNA (Fig. 5A). In total, we altered 422 of 1,176 bases of the TXNIP CDS without changing the TXNIP primary amino acid sequence. We observed that TXNIP-WT and TXNIP-MUT mRNA levels were comparable in control cells and increased upon Ras activation (Fig. 5B). As expected, we observed that the degradation rates of TXNIP-WT and TXNIP-MUT proteins were similar to each other, since the amino acid sequence remained the same (Fig. 5D). Nevertheless, TXNIP-MUT protein levels were still repressed by Ras^{G12V}, although to a lesser

extent than those of TXNIP-WT (Fig. 5C). This suggests that the translational repression of TXNIP by Ras^{G12V} is unlikely to be mediated by a feature(s) of the primary sequence of the TXNIP mRNA, such as mRNA secondary structure, microRNAs (miRNAs), or sequence-specific RNA binding proteins.

The WT TXNIP mRNA is comprised of a significant number of suboptimal codons and even some rare codons. Therefore, we speculated that WT TXNIP mRNA might be at a competitive disadvantage for limited translation machinery in cells where Ras^{G12V} drives global translation. We again used gene synthesis to generate an artificial TXNIP mRNA, TXNIP-OPT. In this case, TXNIP-OPT retains the coding capacity of the TXNIP-WT mRNA, but with suboptimal codons replaced with codons that are most frequently used. In total, we altered 240 of 1,176 bases (Fig. 5A). We observed that TXNIP-OPT mRNA was transcribed similarly to TXNIP-WT mRNA (Fig. 5B) and that the degradation rate of TXNIP-OPT protein was similar to that of TXNIP-WT protein, as expected (Fig. 5D). The amount of TXNIP protein encoded by the TXNIP-OPT mRNA was much greater than that encoded by the TXNIP-WT mRNA, suggesting that the use of high-frequency codons increased the translation efficiency of the TXNIP-OPT mRNA. However, TXNIP-OPT was still subject to translational suppression by Ras^{G12V} (Fig. 5C). This finding suggests that Ras activation does not suppress translation of the TXNIP mRNA simply because it contains suboptimal or even rare codons. Further, the high level of mutation in the TXNIP-OPT mRNA also supports a model in which the primary mRNA sequence is not targeted by Ras^{G12V}.

Ras^{G12V} inhibits TXNIP translation elongation independently of TXNIP's mRNA primary sequence. Next, we investigated whether the primary sequence of the TXNIP mRNA is involved in elongation repression by Ras^{G12V}. To test this, we examined the elongation rates of TXNIP-WT, -MUT, and -OPT messages with and without Ras activation using polysome profiling and a ribosome runoff assay (Fig. 6A). In the absence of harringtonine, the amounts of mRNA of each TXNIP variant that associated with heavy polysomes were similar in control and Ras^{G12V}-expressing cells. Harringtonine treatment caused a decrease in the amount of each TXNIP message associated with heavy polysomes in both cell types. However, the decrease of each TXNIP message was less in Ras^{G12V}-expressing cells than in control cells. Similar to the previous polysome experiment, these results suggest that Ras activation slows the ribosome elongation rates of all three TXNIP messages (Fig. 6B to D). We also observed that ribosomes were cleared less efficiently from the TXNIP-OPT message (24% decrease) than from the TXNIP-WT message (32% decrease) in Ras^{G12V}-expressing cells (Fig. 6B and D). As a control, actin mRNA exhibited equally efficient ribosome clearance in control and Ras^{G12V}-expressing cells (Fig. 6E). These results further support a model in which Ras^{G12V} suppresses translation elongation of the TXNIP mRNA independently of its primary sequence or codon usage.

TXNIP N-terminal peptide sequence mediates translational repression by Ras^{G12V}. Together, our results suggest that a feature of the TXNIP protein sequence is targeted by Ras. Therefore, we investigated which region of the TXNIP protein is necessary or sufficient for translational repression by Ras^{G12V}. To achieve this goal, we fused different regions of TXNIP to dsLuc (Fig. 7A). As described above (Fig. 2G), Ras^{G12V} did not affect the accumulation of dsLuc activity but completely suppressed the accumulation of full-length TXNIP [TXNIP(1–391)]-dsLuc activity after MG132 treatment (Fig. 7B and C). The N terminus of TXNIP is comprised of two related domains, each forming a β-sandwich domain comprised of β-strands (34). We initially examined TXNIP(1–156), which contains only the first β-sandwich domain. Ras^{G12V} partially suppressed the accumulation of TXNIP(1–156)-dsLuc activity (Fig. 7D). Further, TXNIP(1–156)-dsLuc protein did not increase in Ras^{G12V}-expressing cells (Fig. 7E). The accumulation of TXNIP(1–87)-dsLuc activity and protein was completely blocked by Ras activation, suggesting a critical role for the first 87 amino acids of TXNIP in Ras^{G12V}-dependent translational repression (Fig. 7F and G). TXNIP(88–391)-dsLuc activity was only partially sensitive to Ras^{G12V} suppression. Further, Ras^{G12V} did not affect TXNIP(88–391)-dsLuc accumulation, suggesting its synthesis is not blocked by Ras^{G12V} (Fig. 7H

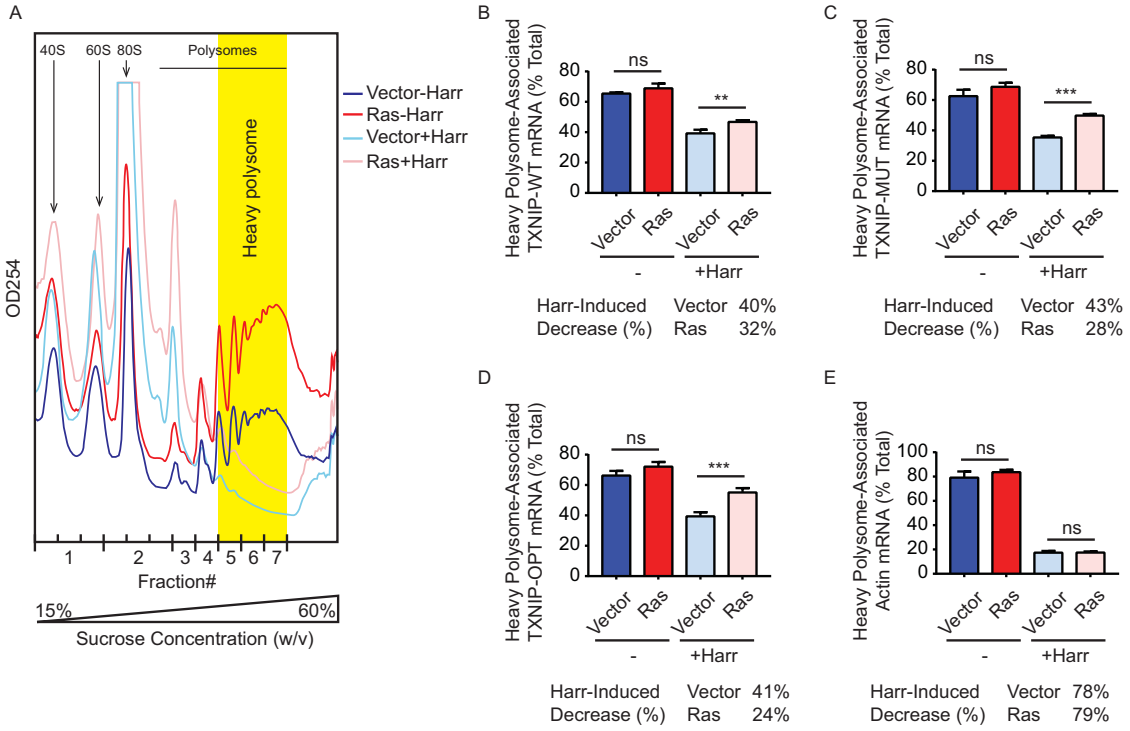

FIG 6 Ras^{G12V} inhibits TXNIP translation elongation independently of TXNIP's mRNA primary sequence. (A) Chromatograms showing the polysome profiles of MondoA KO::TXNIP::Vector (Vector) or Ras^{G12V} (Ras) MEFs before (−Harr) and after (+Harr) harringtonine treatment. Fraction numbers are shown on the *x* axis, with heavy-polysome fractions shaded in yellow. (B to E) RT-qPCR was used to determine the amounts of TXNIP-WT mRNA (B), TXNIP-MUT mRNA (C), TXNIP-OPT mRNA (D), and actin mRNA (E) from heavy-polysome fractions of the listed cell population. The amounts of heavy-polysome-associated mRNAs were normalized to that of total RNA. The percent decrease in heavy-polysome-associated RNA levels caused by harringtonine treatment was calculated for each cell line. Experiments were repeated twice, and a representative experiment is shown. Values are reported as means and SD. Statistical significance was determined using one-way ANOVA. **, $P < 0.01$; ***, $P < 0.001$; ns, $P \geq 0.05$.

and I). As described above (Fig. 2I), the baseline level of each TXNIP-dsLuc chimera was generally higher in Ras^{G12V}-expressing cells than in control cells, likely due to higher transfection efficiency of Ras^{G12V}-expressing cells than control cells (Fig. 7E, G, I, K, and L). Together, these data support our model, in which the first 87 amino acids are sufficient for translational repression by Ras^{G12V}.

To test the potential contribution of the mRNA primary sequence and/or codon frequency in this context, we fused artificial TXNIP mRNAs that comprise the N-terminal 87 amino acids encoded by the MUT or OPT TXNIP sequences to dsLuc (Fig. 5A and 7A). Consistent with our previous finding showing that Ras^{G12V} targets the TXNIP protein sequence, the activities of TXNIP(1–87)-MUT–dsLuc and TXNIP(1–87)-OPT–dsLuc in response to MG132 treatment were both repressed by Ras^{G12V} (Fig. 7J). Further, TXNIP(1–87)-MUT–dsLuc and TXNIP(1–87)-OPT–dsLuc proteins increased in control cells whereas they failed to accumulate in Ras^{G12V}-expressing cells over the course of MG132 treatment (Fig. 7K and L).

DISCUSSION

Our laboratory previously showed that acute growth factor signaling leads to dramatic and rapid suppression of TXNIP expression. In that study, the reduction in TXNIP protein preceded the reduction in TXNIP mRNA, suggesting that growth factor signaling impacts TXNIP protein synthesis and/or degradation (27). In this study, we showed that Ras activation suppresses TXNIP mRNA and protein expression. By bypassing transcriptional regulation, we showed that Ras actively represses translation elongation of TXNIP mRNA. Translating ribosomes continue to transit the TXNIP message (Fig. 3 and 6), albeit at a lower rate in the presence of Ras activation; therefore, we suggest that Ras^{G12V} lowers the rate of elongation rather than causing ribosome stalling.

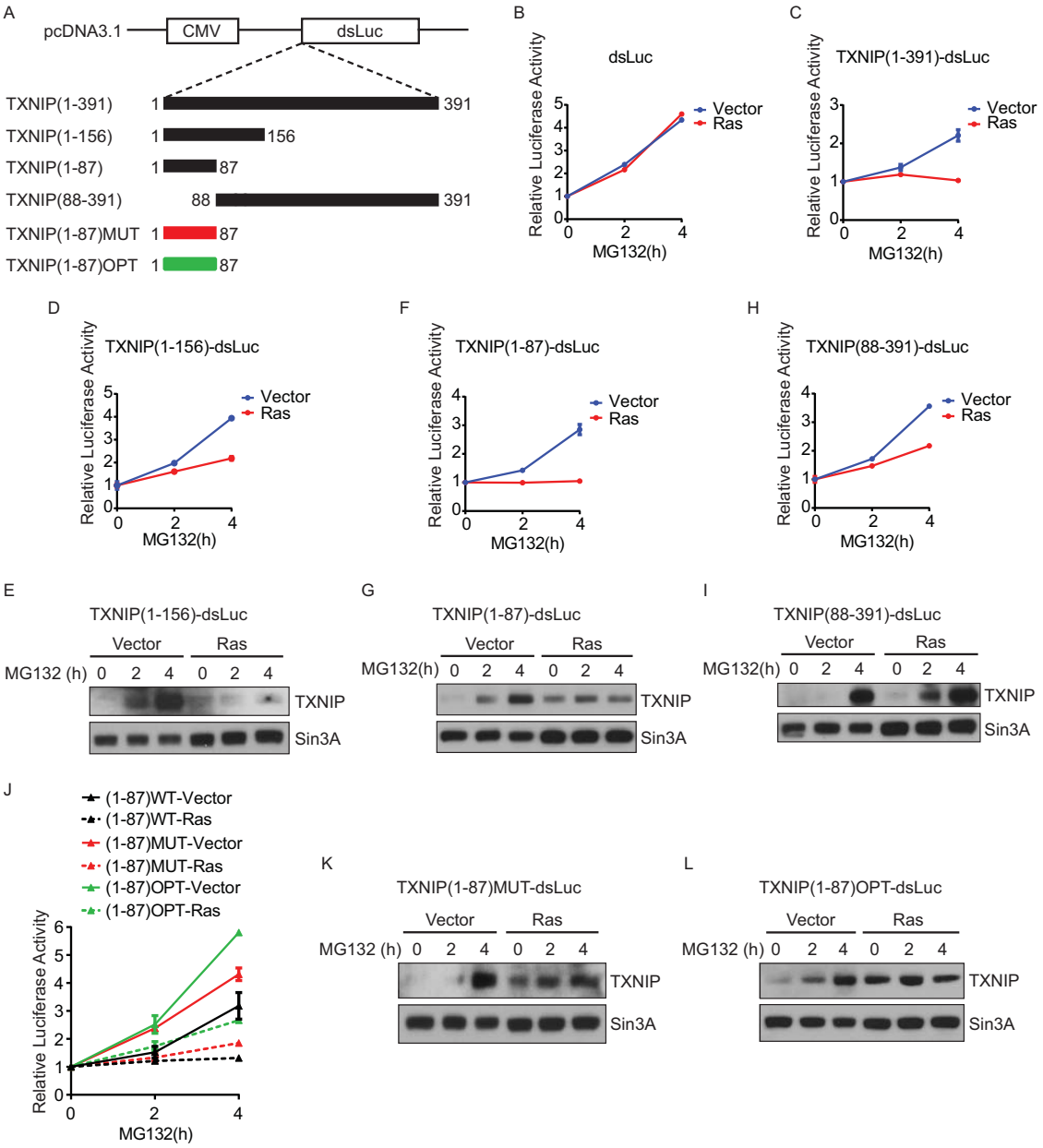

FIG 7 The TXNIP N-terminal peptide sequence mediates translational repression by Ras^{G12V}. (A) Diagram showing luciferase reporter constructs, in which the human full-length TXNIP(1–391), TXNIP(1–156), TXNIP(1–87), TXNIP(88–391), TXNIP(1-87)-MUT, or TXNIP(1-87)-OPT was cloned upstream of and in frame with the destabilized luciferase ORF (dsLuc). (B to L) Luciferase reporters were transfected into MondoA KO::TXNIP::Vector (Vector) or Ras^{G12V} (Ras) MEFs. (B to D, F, H, and J) Relative luciferase activity, normalized to β-Gal activity, of each reporter was determined following a time course of treatment with 20 μM MG132 in the indicated cell lines. The luciferase experiments were repeated at least twice, and representative experiments are shown. Values are reported as means and SD. (E, G, I, K, and L) Western blotting was used to determine the levels of the indicated proteins following a time course of treatment with 20 μM MG132 in the indicated cell lines.

Ras activation also stimulates TXNIP turnover, but this mechanism accounts for only a fraction (~25%) of the effect of Ras activation on TXNIP levels: the repression of TXNIP synthesis accounts for the majority of the remaining Ras-dependent decrease in TXNIP (Fig. 2). Ras activation represses transcription of the TXNIP gene and controls TXNIP levels posttranscriptionally by inducing degradation of the TXNIP protein and blocking translation elongation of the TXNIP message. We speculate that this multifaceted downregulation of TXNIP expression by activated Ras helps ensure that adequate glucose is available to support Ras-driven anabolic biosynthetic pathways.

Growth factor signaling is known to promote global protein synthesis through upregulation of translation initiation and elongation (30, 31); therefore, it is striking that Ras activation blocks translation elongation of the TXNIP message. We showed that, like growth factor signaling, Ras^{G12V} upregulates global protein synthesis in MEFs (Fig. 3A). However, Ras activation blocks TXNIP synthesis. Our analysis of published polysome profiling data suggests that messages with elongation dynamics similar to those of TXNIP do not generally encode growth/tumor suppressors (Fig. 4). This finding suggests that Ras^{G12V}-mediated translational inhibition might be restricted to TXNIP or a smaller set of messages.

We next investigated the mechanisms by which Ras^{G12V} specifically downregulates the translation of TXNIP mRNA. The artificial TXNIP mRNAs, TXNIP-MUT and TXNIP-OPT, are both significantly different from TXNIP-WT in primary sequence. TXNIP-MUT is designed to alter the coding sequence without changing the overall codon usage frequency. Ras activation suppresses TXNIP expression when it is encoded by TXNIP-MUT. Therefore, we propose that Ras regulates TXNIP synthesis by a mechanism independent of the mRNA primary sequence. TXNIP-OPT is designed with optimal codon usage, i.e., with increased usage of high-frequency codons, which positively impacts the elongation rate (35–38). TXNIP-OPT is still subject to Ras^{G12V}-dependent translational repression, suggesting that suboptimal codon usage in the TXNIP message is not responsible for the translational repression by Ras^{G12V}. Supporting our model, in which the primary sequence of the TXNIP mRNA is not targeted by Ras^{G12V}, the rate at which ribosomes elongate on TXNIP-MUT and TXNIP-OPT mRNAs is lower in the presence of Ras^{G12V}. Together, these experiments suggest that Ras does not require the primary sequence of the TXNIP mRNA to repress TXNIP synthesis.

The amount of TXNIP protein is greater when it is encoded by the TXNIP-OPT message than when it is encoded by the TXNIP-WT message, most likely due to its increased translation efficiency (Fig. 5). The expectation for a message translated with high efficiency is high ribosome occupancy and a high elongation rate. Paradoxically, in control cells, similar numbers of ribosomes seem to bind to TXNIP-WT and TXNIP-OPT messages, and ribosomes are cleared from both messages similarly (Fig. 6B and D). There are at least two possibilities that may account for the paradox. First, it is possible that the limited resolution of the F7 polysome fraction, which likely comprises mRNA with a high and potentially variable number of ribosomes, masks increased ribosome occupancy on the TXNIP-OPT message. Nonetheless, in Ras^{G12V}-expressing cells, ribosomes are cleared from the TXNIP-OPT message less efficiently than from the TXNIP-WT message. These data suggest that TXNIP-OPT mRNA associates with more ribosomes than TXNIP-WT mRNA, which is consistent with its higher translation efficiency.

Second, it is possible that the protein expression level does not necessarily correlate with the elongation rate of any given message. We examined the correlation between the elongation rate, using the "ribosome retention ratio" (as shown in Fig. 4F), and the GC3 bias, which has been shown to a good indicator of the protein expression level (39–41). Supporting this idea, we observed a very weak correlation between these two variables (data not shown). Based on this analysis, we suggest that high protein expression of TXNIP-OPT is not necessarily related to a higher elongation rate or higher ribosome density of its message. A higher-resolution approach is required to determine whether these models, and potentially others, can explain why the TXNIP-WT and -OPT messages appear to show similar ribosome occupancies.

In contrast to the lack of involvement of the sequence of TXNIP mRNA, we discovered that the N terminus of the TXNIP protein is necessary and sufficient for translational repression by Ras^{G12V}. We note that the effect of deleting the N terminus of TXNIP is only partial (Fig. 7H), suggesting that other regions of TXNIP also contribute to the Ras-dependent blockade of TXNIP synthesis. Using TXNIP truncation variants, TXNIP(1–87)-MUT and TXNIP(1–87)-OPT, we showed again that the peptide sequence rather than the mRNA sequence encoding the first 87 amino acids is required for translational repression. These data suggest that activated Ras targets the N terminus of TXNIP as it exits the ribosome, resulting in a decreased rate of translation elongation

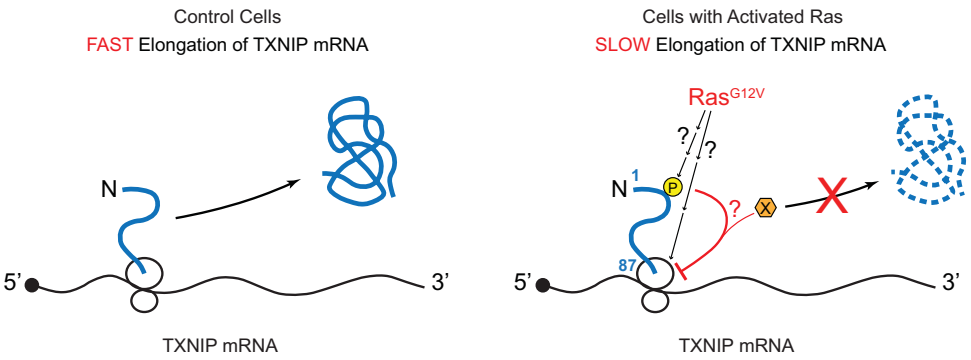

FIG 8 RasG12V suppresses TXNIP translation elongation. In unstimulated cells, a significant amount of TXNIP protein is synthesized from fast translation elongation of the TXNIP mRNA. In Ras-activated cells, TXNIP synthesis is suppressed due to the reduced rate at which ribosomes translate the TXNIP mRNA via a mechanism(s) that involves the nascent peptide of the TXNIP N terminus. The first 87 amino acids of the TXNIP protein or the ribosome itself (ribosomal proteins or rRNAs) might be targeted by Ras-dependent posttranslational modifications, which impede peptide release, leading to slow elongation.

(Fig. 8). The dependence on the N terminus of TXNIP for Ras-dependent repression is consistent with our contention that the blockade of translation elongation by Ras may be restricted to TXNIP or to a small group of proteins that show homology to the TXNIP N terminus.

We observed two prominent peaks along the TXNIP CDS corresponding to amino acids 66 and 81 of the TXNIP protein (Fig. 4D), which is an indication of high ribosome density and potentially slow ribosome translocation. We propose that the slow elongation dynamics in this region of the TXNIP mRNA provides an opportunity for cotranslational regulation by RasG12V. We examined the ribosome distribution on ARRDC4 transcript, which is a TXNIP paralog with high conservation in the N terminus that is also a potent negative regulator of glucose uptake (42). Interestingly, ARRDC4 transcript also shows high ribosome density at the position corresponding to amino acid 85 of the ARRDC4 protein (data not shown), suggesting that its translation may also be regulated by Ras.

RasG12V targets the N terminus of TXNIP, but we do not yet understand how that impacts translation elongation. Accumulating evidence suggests that the nascent peptide chain regulates translation elongation by peptide sequence-specific interaction with the ribosome exit tunnel, which is accompanied by stalled ribosomal complexes (43–50). In addition, cotranslational modification of the protein being translated can regulate protein synthesis (51, 52). Given these findings, it is possible that RasG12V modifies the nascent peptide chain of the TXNIP N terminus, likely indirectly, to impede the peptide release and the elongation dynamics (Fig. 8). Consistent with this idea, TXNIP harbors a number of conserved sites for potential posttranslational modification within its first 87 amino acids. A second possibility is based on the observation that modifications of ribosomal proteins and rRNAs regulate translation in a growth phase-dependent manner and in response to environmental signals (53, 54). Therefore, it is also possible that RasG12V targets the ribosome itself, thereby affecting its interaction with the nascent peptide chain of the TXNIP N terminus to achieve a specific blockade of TXNIP elongation (Fig. 8). Additional studies will be necessary to test these models and others. Our preliminary studies suggest that canonical Ras effector pathways do not block TXNIP translation (data not shown). Thus, Ras may drive metabolic reprogramming toward aerobic glycolysis by regulating translation elongation of the TXNIP mRNA, and potentially other messages, via a novel effector pathway.

MATERIALS AND METHODS

Cell culture and conditions. All cells were maintained at 37°C in 5% CO_2 in Dulbecco's modified Eagle's medium (DMEM) (Gibco; no. 11995-065) supplemented with 10% fetal bovine serum (FBS) (Gibco; no. 26140-079) and 1% penicillin-streptomycin (Gibco; no. 15140-122). Wild-type and MondoA KO MEFs

were generated in the laboratory as described previously (23). The MEFs were immortalized with simian virus 40 (SV40) large T antigen.

Plasmids and virus infection. The retroviral constructs pBabePuro and pBabePuro-H-Ras^{G12V} were gifts from S. Lessnick. Human TXNIP variants (TXNIP-WT, -MUT, and -OPT) were cloned into the pWzlBlast retroviral vector. TXNIP-MUT and TXNIP-OPT were generated by gBlocks gene fragments (Integrated DNA Technologies) and Gibson cloning (NEB; no. E2621L). The sequences of TXNIP-MUT and TXNIP-OPT are available upon request. Retroviruses of each construct were packaged in HEK293EBNA cells with vesicular stomatitis virus G (VSVG) and gag-pol plasmids. Stable cell lines were generated by retroviral infection followed by antibiotic selection (2 μg/ml puromycin for pBabePuro constructs; 3.5 μg/ml blasticidin for pWzlBlast constructs).

Relative codon adaptiveness. Relative codon adaptiveness for TXNIP-WT, -MUT, and -OPT was calculated against a mouse codon usage table and plotted using a Web-based graphical codon usage analyzer (http://gcua.schoedl.de/sequential_v2.html).

Chemicals and reagents. For proteasome inhibition, 20 μM MG132 (Calbiochem; no. 474790) was used for the indicated times. For protein synthesis inhibition, 40 μg/ml cycloheximide (Sigma; no. C7698) was used for the indicated times. For ribosome runoff assays, cells were treated with 2 μg/ml harringtonine (Cayman Chemical; no. 15361) for 10 min.

Western blotting. Whole-cell lysate was prepared in ice-cold lysis buffer (400 mM NaCl, 20 mM HEPES [pH 7.6], 0.1% NP-40, 25% glycerol, 1 mM EDTA, 1 mM EGTA, 1 mM dithiothreitol [DTT]) containing protease inhibitors (1 mM phenylmethylsulfonyl fluoride [PMSF], 2.5 μg/ml aprotinin, 1 μg/ml leupeptin, 1 μg/ml pepstatin) and phosphatase inhibitors (phosphatase inhibitor cocktails 1 and 2; Sigma; no. P2850 and P5726). The protein concentration was determined by Bio-Rad protein assay (Bio-Rad; no. 500-0006). The same amount of protein for individual samples was resolved on SDS-PAGE, transferred to polyvinylidene difluoride (PVDF) membranes, and subsequently blocked in 5% nonfat milk in TBST (1× Tris-buffered saline with 0.1% Tween 20), followed by probing with primary antibodies at 1:2,000 dilution overnight at 4°C, as follows: MLXIP/MondoA, Proteintech no. 13614-1-AP; TXNIP, Abcam no. ab188865; TXNIP(JY1), MBL Life Science no. K0204-3 [used only for detection of TXNIP(88–391)-dsLuc]; H-Ras(c-20), Santa Cruz no. sc-520; c-Myc(Y69), Abcam no. ab32072. Horseradish peroxidase (HRP)-conjugated mouse IgG (1:5,000; GE Healthcare; no. NA931V) or rabbit IgG (1:15,000; GE Healthcare; no. NA934V) and Western Lightning Plus-ECL (PerkinElmer; no. NEL104001EA) were used for signal detection. Experiments were repeated at least twice, and representative experiments are shown.

Click assay. Cells were cultured with complete medium lacking methionine (−Met) (1× DMEM without L-Gln and L-Met [MP Biomedicals; no. 1642254] supplemented with 4 mM glutamine and 2% FBS) for 1 h prior to AHA labeling. MG132 (20 μM) was added to the −Met medium 30 min before AHA labeling. AHA (Invitrogen; no. C10102) was then added to the −Met medium at a final concentration of 50 μM, and the cells were labeled for the indicated times. Whole-cell lysate was prepared in ice-cold radioimmunoprecipitation assay (RIPA) buffer (50 mM Tris-HCl [pH 7.4], 150 mM NaCl, 1% NP-40, 0.1% SDS, 0.25% Na deoxycholate) containing protease inhibitors (1 mM PMSF, 2.5 μg/ml aprotinin, 1 μg/ml leupeptin, and 1 μg/ml pepstatin) and phosphatase inhibitors (50 mM NaF, 10 mM β-glycerophosphate, and 1.5 mM Na_3VO_4). The protein concentration was determined by detergent-compatible protein assay (Bio-Rad; no. 500-0112). Lysate (100 μg) was subjected to a click reaction using biotin alkyne (Invitrogen; no. B10185) and a Click-iT protein reaction buffer kit (Invitrogen; no. C10276) overnight at 4°C, following the manufacturer's protocol.

For measurement of global protein synthesis, the same volume of reacted lysate was analyzed by Western blotting with HRP-conjugated streptavidin (1:2,000; GE Healthcare; no. RPN1231V). For measurement of the TXNIP protein synthesis rate, the reacted lysate was chloroform-methanol (MeOH) precipitated and resuspended in resolubilization buffer (60 mM Tris [pH 6.8], 1% SDS, 10% glycerol). The protein concentration was determined using a detergent-compatible protein assay. The resolubilized lysates (7.5 μg) were subjected to streptavidin (SA) affinity purification in RIPA buffer at 4°C overnight. The same amount of lysate (with an equivalent amount of SA affinity-purified samples as the input) was subjected to Western blotting. Experiments were repeated at least twice, and representative experiments are shown.

Luciferase reporter assay. pcDNA3.1dsLuc2CP (dsLuc) was purchased from Addgene (no. 68054). TXNIP(1–391), TXNIP(1–87)-WT, TXNIP(1–87)-MUT, TXNIP(1–87)-OPT, and TXNIP(88–391) were PCR amplified from the respective pWzlBlast-TXNIP (WT, MUT, or OPT) constructs (as described above) with specific primers with 25-bp overhangs and subsequently cloned upstream of and in frame with dsLuc in the pcDNA3.1dsLuc2CP plasmid by Gibson cloning. Transfections were performed 24 h after cell plating, when the cell monolayers were 60 to 70% confluent. The cells were treated with 40 μg/ml CHX or 20 μM MG132 for the indicated times 22 to 24 h posttransfection and harvested in reporter lysis buffer (Promega; no. E397A). Luciferase reporter assays were performed as previously described (55). Luciferase activity was normalized to β-galactosidase (β-Gal) activity and presented as a value relative to that at 0 h for both MG132 and CHX experiments. Experiments were repeated at least twice, and representative experiments are shown. Values are reported as means and standard deviations (SD) of three technical replicates. The same volume of lysates in reporter lysis buffer was subjected to Western blotting for validation of the protein expression of the indicated constructs under the listed conditions.

RT-qPCR. Total RNA was extracted using a Quick-RNA miniprep kit (Zymo Research). cDNA was generated from 100 to 300 ng RNA using a GoScript reverse transcription kit (Promega). qPCR was performed using a CFX Connect real-time system and CFX manager software (Bio-Rad). Relative mRNA expression levels were determined from standard curves for each primer set and were normalized to β-actin expression. Experiments were repeated at least twice, and representative experiments are shown.

Values were reported as means and SD of three technical replicates. Statistical significance was determined using *t* tests. RT primer sequences are available upon request.

Polysome profiling. Sucrose gradients (10% to 50% or 15% to 60% [wt/vol]) in gradient buffer (15 mM Tris [pH 7.4], 15 mM $MgCl_2$, 100 mM KCl, 1 mM DTT, 100 μg/ml CHX) were prepared in 5-ml ultracentrifuge tubes (Beckman; no. 326819) the night before an experiment and stored at 4°C. Cells were washed and incubated with ice-cold phosphate-buffered saline (PBS) containing 100 μg/ml CHX for 2 min. The cells were scraped into Eppendorf tubes and centrifuged at 2,000 $\times$ *g* for 4 min at 4°C. The cell pellet was collected and lysed in polysome lysis buffer (15 mM Tris [pH 7.4], 15 mM $MgCl_2$, 100 mM KCl, 1% Triton X-100, 1 mM DTT, 100 μg/ml CHX, 500 U/ml SuperaseIn [Invitrogen; no. AM2696]) containing protease inhibitors (1 mM PMSF, 2.5 μg/ml aprotinin, 1 μg/ml leupeptin, 1 μg/ml pepstatin) and phosphatase inhibitors (phosphatase inhibitor cocktails 1 and 2; Sigma; no. P2850 and P5726). The cell lysate was loaded onto the top of a sucrose gradient and centrifuged at 47,000 rpm for 1 h at 4°C in a SW55 Ti rotor (Beckman; no. 342194), and centrifugation was stopped with no brake. The centrifuged sample was fractionated with a syringe pump coupled with a UA-6 detector that continuously monitored the OD_{254} values (Teledyne ISCO), and 250-μl fractions were collected from the beginning of the 40S peak toward the end of the gradient. After fractionation, fractions corresponding to 40S, 60S, and 80S peaks were combined, and fraction numbers were assigned (Fig. 3B and 6A show the fraction numbers on the *x* axis). The same volume of each fraction was taken and supplemented with 0.1 ng of luciferase mRNA (Promega), which served as a spike-in control. RNA was extracted using TRIzol LS reagent (Invitrogen) and a Direct-zol RNA miniprep kit (Zymo Research). cDNA was synthesized from the same volume of RNA using a GoScript reverse transcription kit (Promega). Levels of genes of interest were determined by RT-qPCR. The data were normalized to the luciferase RNA level to account for differences in RNA extraction and cDNA synthesis. The total RNA level was calculated by summing the qPCR values from each fraction across the entire gradient; the qPCR values from heavy-polysome fractions were combined and presented as percent total RNA (Fig. 3B and 6A). Experiments were repeated twice, and representative experiments are shown. Values were reported as means and SD of three technical replicates. Statistical significance was determined using one-way analysis of variance (ANOVA).

For polysome profiling of cells expressing TXNIP-WT, -MUT, or -OPT (Fig. 6), each cell line (MondoA KO::TXNIP-WT::Vector, -MUT::Vector, -OPT::Vector, -WT::Ras^{G12V}, -MUT::Ras^{G12V}, or -OPT::Ras^{G12V}) for each treatment group (without [−Harr] or with [+Harr] harringtonine) was plated and treated individually. During harvest, control cells with different TXNIP variants (WT, MUT, or OPT) from the same treatment group were pooled (Vector−Harr or Vector+Harr). Similarly, Ras^{G12V}-expressing cells with different TXNIP variants (WT, MUT, or OPT) from the same treatment group were pooled (Ras−Harr or Ras+Harr). The sample-pooling method was used to ensure identical experimental conditions. The resulting four samples were subjected to polysome profiling and subsequent analysis to determine the RNA levels of genes of interest.

Informatics. Gene expression values (mRNA expression Z-scores) of TXNIP and H-Ras-dependent genes (56) were obtained for the breast cancer (METABRIC) (57), lung adenocarcinoma (TCGA) (58), and pancreatic adenocarcinoma (TCGA, provisional) data sets available on cBioPortal (59, 60; http://www.cbioportal.org/). For the H-Ras gene signature, the Z-scores of the H-Ras signature genes were subjected to principal-component analysis (PCA) using the prcomp function in R (https://www.r-project.org/). The values of principal component 2 were used as the H-Ras gene signature for each tumor sample.

Ribosome profiling data were obtained from the Gene Expression Omnibus (GEO) (accession number GSE30839): 0-s harringtonine treatment sample, GSM765292; 120-s harringtonine treatment sample, GSM765294 (33). Sequencing data were preprocessed and aligned on the Galaxy server with the published method (61). To directly compare ribosome occupancies of mRNA transcripts across the entire genome, the gene transcript length was normalized to 100 bins, and the relative ribosome density (percent total reads from 100 bins) for each bin was calculated. The data are presented as relative ribosome density (*y* axis) against normalized CDS length (*x* axis). The elongation profile of each gene transcript was generated by calculating the difference in the relative ribosome density caused by harringtonine treatment for each bin across the CDS. Unsupervised clustering was performed for the top 9,962 translationally active gene transcripts based on their elongation profiles using the Cluster 3.0 program. The clustering result was visualized in a heat map using the TreeView program, in which red indicates an increase in the relative ribosome density upon harringtonine treatment and green indicates a decrease in the relative ribosome density upon harringtonine treatment. The ribosome retention ratio (RRR) was calculated as the percentage of the cumulative relative ribosome density of the last 90 bins for each transcript in harringtonine-treated samples. An RRR value closer to 0 indicates a higher elongation rate, whereas an RRR value closer to 1 indicates a lower elongation rate. The lists of oncogenes and tumor suppressors were obtained from the UniProt database. The ribosome retention ratio of each gene was plotted as a grouped scatter plot, with the median and interquartile range indicated on the graph.

ACKNOWLEDGMENTS

We thank the Weyrich laboratory for providing equipment and help for the polysome profiling experiments, the members of the Ayer laboratory for helpful discussion and insights, and Betty Leibold for comments on the manuscript.

This work was supported by grants from the NIH (R01 GM055668-14A1) and the Department of Defense (BC133708) to D.E.A. The research reported in this publication utilized the High-Throughput Genomics and Bioinformatics Core at Hunts-

man Cancer Institute at the University of Utah and was supported by the National Cancer Institute of the National Institutes of Health under award number P30CA042014. The research reported in this publication was supported by the Huntsman Cancer Foundation.

The content is solely our responsibility and does not necessarily represent the official views of the NIH.

REFERENCES

1. Bos JL. 1989. *ras* oncogenes in human cancer: a review. Cancer Res 49:4682–4689.
2. Rajalingam K, Schreck R, Rapp UR, Albert S. 2007. Ras oncogenes and their downstream targets. Biochim Biophys Acta 1773:1177–1195. https://doi.org/10.1016/j.bbamcr.2007.01.012.
3. Hu Y, Lu W, Chen G, Wang P, Chen Z, Zhou Y, Ogasawara M, Trachootham D, Feng L, Pelicano H, Chiao PJ, Keating MJ, Garcia-Manero G, Huang P. 2012. K-ras(G12V) transformation leads to mitochondrial dysfunction and a metabolic switch from oxidative phosphorylation to glycolysis. Cell Res 22:399–412. https://doi.org/10.1038/cr.2011.145.
4. Gaglio D, Metallo CM, Gameiro PA, Hiller K, Danna LS, Balestrieri C, Alberghina L, Stephanopoulos G, Chiaradonna F. 2011. Oncogenic K-Ras decouples glucose and glutamine metabolism to support cancer cell growth. Mol Syst Biol 7:523. https://doi.org/10.1038/msb.2011.56.
5. Chiaradonna F, Sacco E, Manzoni R, Giorgio M, Vanoni M, Alberghina L. 2006. Ras-dependent carbon metabolism and transformation in mouse fibroblasts. Oncogene 25:5391–5404. https://doi.org/10.1038/sj.onc.1209528.
6. Hu CJ, Wang LY, Chodosh LA, Keith B, Simon MC. 2003. Differential roles of hypoxia-inducible factor 1alpha (HIF-1alpha) and HIF-2alpha in hypoxic gene regulation. Mol Cell Biol 23:9361–9374. https://doi.org/10.1128/MCB.23.24.9361-9374.2003.
7. Kim JW, Zeller KI, Wang Y, Jegga AG, Aronow BJ, O'Donnell KA, Dang CV. 2004. Evaluation of myc E-box phylogenetic footprints in glycolytic genes by chromatin immunoprecipitation assays. Mol Cell Biol 24:5923–5936. https://doi.org/10.1128/MCB.24.13.5923-5936.2004.
8. Osthus RC, Shim H, Kim S, Li Q, Reddy R, Mukherjee M, Xu Y, Wonsey D, Lee LA, Dang CV. 2000. Deregulation of glucose transporter 1 and glycolytic gene expression by c-Myc. J Biol Chem 275:21797–21800. https://doi.org/10.1074/jbc.C000023200.
9. Ying H, Kimmelman AC, Lyssiotis CA, Hua S, Chu GC, Fletcher-Sananikone E, Locasale JW, Son J, Zhang H, Coloff JL, Yan H, Wang W, Chen S, Viale A, Zheng H, Paik JH, Lim C, Guimaraes AR, Martin ES, Chang J, Hezel AF, Perry SR, Hu J, Gan B, Xiao Y, Asara JM, Weissleder R, Wang YA, Chin L, Cantley LC, DePinho RA. 2012. Oncogenic Kras maintains pancreatic tumors through regulation of anabolic glucose metabolism. Cell 149:656–670. https://doi.org/10.1016/j.cell.2012.01.058.
10. Wu N, Zheng B, Shaywitz A, Dagon Y, Tower C, Bellinger G, Shen CH, Wen J, Asara J, McGraw TE, Kahn BB, Cantley LC. 2013. AMPK-dependent degradation of TXNIP upon energy stress leads to enhanced glucose uptake via GLUT1. Mol Cell 49:1167–1175. https://doi.org/10.1016/j.molcel.2013.01.035.
11. Waldhart AN, Dykstra H, Peck AS, Boguslawski EA, Madaj ZB, Wen J, Veldkamp K, Hollowell M, Zheng B, Cantley lc, mcgraw te, wu n. 2017. phosphorylation of txnip by akt mediates acute influx of glucose in response to insulin. Cell Rep 19:2005–2013. https://doi.org/10.1016/j.celrep.2017.05.041.
12. Parikh H, Carlsson E, Chutkow WA, Johansson LE, Storgaard H, Poulsen P, Saxena R, Ladd C, Schulze PC, Mazzini MJ, Jensen CB, Krook A, Bjornholm M, Tornqvist H, Zierath JR, Ridderstrale M, Altshuler D, Lee RT, Vaag A, Groop LC, Mootha VK. 2007. TXNIP regulates peripheral glucose metabolism in humans. PLoS Med 4:e158. https://doi.org/10.1371/journal.pmed.0040158.
13. Chutkow WA, Patwari P, Yoshioka J, Lee RT. 2008. Thioredoxin-interacting protein (Txnip) is a critical regulator of hepatic glucose production. J Biol Chem 283:2397–2406. https://doi.org/10.1074/jbc.M708169200.
14. Hui ST, Andres AM, Miller AK, Spann NJ, Potter DW, Post NM, Chen AZ, Sachithanantham S, Jung DY, Kim JK, Davis RA. 2008. Txnip balances metabolic and growth signaling via PTEN disulfide reduction. Proc Natl Acad Sci U S A 105:3921–3926. https://doi.org/10.1073/pnas.0800293105.
15. Stoltzman CA, Peterson CW, Breen KT, Muoio DM, Billin AN, Ayer DE. 2008. Glucose sensing by MondoA:Mlx complexes: a role for hexokinases and direct regulation of thioredoxin-interacting protein expression. Proc Natl Acad Sci U S A 105:6912–6917. https://doi.org/10.1073/pnas.0712199105.
16. Chutkow WA, Birkenfeld AL, Brown JD, Lee HY, Frederick DW, Yoshioka J, Patwari P, Kursawe R, Cushman SW, Plutzky J, Shulman GI, Samuel VT, Lee RT. 2010. Deletion of the alpha-arrestin protein Txnip in mice promotes adiposity and adipogenesis while preserving insulin sensitivity. Diabetes 59:1424–1434. https://doi.org/10.2337/db09-1212.
17. DeBalsi KL, Wong KE, Koves TR, Slentz DH, Seiler SE, Wittmann AH, Ilkayeva OR, Stevens RD, Perry CG, Lark DS, Hui ST, Szweda L, Neufer PD, Muoio DM. 2014. Targeted metabolomics connects thioredoxin-interacting protein (TXNIP) to mitochondrial fuel selection and regulation of specific oxidoreductase enzymes in skeletal muscle. J Biol Chem 289:8106–8120. https://doi.org/10.1074/jbc.M113.511535.
18. Saxena G, Chen J, Shalev A. 2010. Intracellular shuttling and mitochondrial function of thioredoxin-interacting protein. J Biol Chem 285:3997–4005. https://doi.org/10.1074/jbc.M109.034421.
19. Jeon JH, Lee KN, Hwang CY, Kwon KS, You KH, Choi I. 2005. Tumor suppressor VDUP1 increases p27(kip1) stability by inhibiting JAB1. Cancer Res 65:4485–4489. https://doi.org/10.1158/0008-5472.CAN-04-2271.
20. Shen L, O'Shea JM, Kaadige MR, Cunha S, Wilde BR, Cohen AL, Welm AL, Ayer DE. 2015. Metabolic reprogramming in triple-negative breast cancer through Myc suppression of TXNIP. Proc Natl Acad Sci U S A 112:5425–5430. https://doi.org/10.1073/pnas.1501555112.
21. Chen JL, Merl D, Peterson CW, Wu J, Liu PY, Yin H, Muoio DM, Ayer DE, West M, Chi JT. 2010. Lactic acidosis triggers starvation response with paradoxical induction of TXNIP through MondoA. PLoS Genet 6:e1001093. https://doi.org/10.1371/journal.pgen.1001093.
22. Cadenas C, Franckenstein D, Schmidt M, Gehrmann M, Hermes M, Geppert B, Schormann W, Maccoux LJ, Schug M, Schumann A, Wilhelm C, Freis E, Ickstadt K, Rahnenfuhrer J, Baumbach JI, Sickmann A, Hengstler JG. 2010. Role of thioredoxin reductase 1 and thioredoxin interacting protein in prognosis of breast cancer. Breast Cancer Res 12:R44. https://doi.org/10.1186/bcr2599.
23. Peterson CW, Stoltzman CA, Sighinolfi MP, Han KS, Ayer DE. 2010. Glucose controls nuclear accumulation, promoter binding, and transcriptional activity of the MondoA-Mlx heterodimer. Mol Cell Biol 30:2887–2895. https://doi.org/10.1128/MCB.01613-09.
24. O'Shea JM, Ayer DE. 2013. Coordination of nutrient availability and utilization by MAX- and MLX-centered transcription networks. Cold Spring Harb Perspect Med 3:a014258. https://doi.org/10.1101/cshperspect.a014258.
25. Billin AN, Eilers AL, Coulter KL, Logan JS, Ayer DE. 2000. MondoA, a novel basic helix-loop-helix-leucine zipper transcriptional activator that constitutes a positive branch of a max-like network. Mol Cell Biol 20:8845–8854. https://doi.org/10.1128/MCB.20.23.8845-8854.2000.
26. Sans CL, Satterwhite DJ, Stoltzman CA, Breen KT, Ayer DE. 2006. MondoA-Mlx heterodimers are candidate sensors of cellular energy status: mitochondrial localization and direct regulation of glycolysis. Mol Cell Biol 26:4863–4871. https://doi.org/10.1128/MCB.00657-05.
27. Elgort MG, O'Shea JM, Jiang Y, Ayer DE. 2010. Transcriptional and translational downregulation of thioredoxin interacting protein is required for metabolic reprogramming during G(1). Genes Cancer 1:893–907. https://doi.org/10.1177/1947601910389604.
28. Kaadige MR, Yang J, Wilde BR, Ayer DE. 2015. MondoA-Mlx transcriptional activity is limited by mTOR-MondoA interaction. Mol Cell Biol 35:101–110. https://doi.org/10.1128/MCB.00636-14.
29. Zhang P, Wang C, Gao K, Wang D, Mao J, An J, Xu C, Wu D, Yu H, Liu JO, Yu L. 2010. The ubiquitin ligase itch regulates apoptosis by targeting thioredoxin-interacting protein for ubiquitin-dependent degradation. J Biol Chem 285:8869–8879. https://doi.org/10.1074/jbc.M109.063321.

30. Proud CG. 2007. Signalling to translation: how signal transduction pathways control the protein synthetic machinery. Biochem J 403:217–234. https://doi.org/10.1042/BJ20070024.
31. Holland EC, Sonenberg N, Pandolfi PP, Thomas G. 2004. Signaling control of mRNA translation in cancer pathogenesis. Oncogene 23:3138–3144. https://doi.org/10.1038/sj.onc.1207590.
32. Faller WJ, Jackson TJ, Knight JR, Ridgway RA, Jamieson T, Karim SA, Jones C, Radulescu S, Huels DJ, Myant KB, Dudek KM, Casey HA, Scopelliti A, Cordero JB, Vidal M, Pende M, Ryazanov AG, Sonenberg N, Meyuhas O, Hall MN, Bushell M, Willis AE, Sansom OJ. 2015. mTORC1-mediated translational elongation limits intestinal tumour initiation and growth. Nature 517:497–500. https://doi.org/10.1038/nature13896.
33. Ingolia NT, Lareau LF, Weissman JS. 2011. Ribosome profiling of mouse embryonic stem cells reveals the complexity and dynamics of mammalian proteomes. Cell 147:789–802. https://doi.org/10.1016/j.cell.2011.10.002.
34. Hwang J, Suh HW, Jeon YH, Hwang E, Nguyen LT, Yeom J, Lee SG, Lee C, Kim KJ, Kang BS, Jeong JO, Oh TK, Choi I, Lee JO, Kim MH. 2014. The structural basis for the negative regulation of thioredoxin by thioredoxin-interacting protein. Nat Commun 5:2958. https://doi.org/10.1038/ncomms3958.
35. Gingold H, Pilpel Y. 2011. Determinants of translation efficiency and accuracy. Mol Syst Biol 7:481. https://doi.org/10.1038/msb.2011.14.
36. Frenkel-Morgenstern M, Danon T, Christian T, Igarashi T, Cohen L, Hou YM, Jensen LJ. 2012. Genes adopt non-optimal codon usage to generate cell cycle-dependent oscillations in protein levels. Mol Syst Biol 8:572. https://doi.org/10.1038/msb.2012.3.
37. Novoa EM, Ribas de Pouplana L. 2012. Speeding with control: codon usage, tRNAs, and ribosomes. Trends Genet 28:574–581. https://doi.org/10.1016/j.tig.2012.07.006.
38. Quax TE, Claassens NJ, Soll D, van der Oost J. 2015. Codon bias as a means to fine-tune gene expression. Mol Cell 59:149–161. https://doi.org/10.1016/j.molcel.2015.05.035.
39. Lander ES, Linton LM, Birren B, Nusbaum C, Zody MC, Baldwin J, Devon K, Dewar K, Doyle M, FitzHugh W, Funke R, Gage D, Harris K, Heaford A, Howland J, Kann L, Lehoczky J, LeVine R, McEwan P, McKernan K, Meldrim J, Mesirov JP, Miranda C, Morris W, Naylor J, Raymond C, Rosetti M, Santos R, Sheridan A, Sougnez C, Stange-Thomann Y, Stojanovic N, Subramanian A, Wyman D, Rogers J, Sulston J, Ainscough R, Beck S, Bentley D, Burton J, Clee C, Carter N, Coulson A, Deadman R, Deloukas P, Dunham A, Dunham I, Durbin R, French L, Grafham D, et al. 2001. Initial sequencing and analysis of the human genome. Nature 409:860–921. https://doi.org/10.1038/35057062.
40. Shen W, Wang D, Ye B, Shi M, Ma L, Zhang Y, Zhao Z. 2015. GC3-biased gene domains in mammalian genomes. Bioinformatics 31:3081–3084. https://doi.org/10.1093/bioinformatics/btv329.
41. Lampson BL, Pershing NL, Prinz JA, Lacsina JR, Marzluff WF, Nicchitta CV, MacAlpine DM, Counter CM. 2013. Rare codons regulate KRas oncogenesis. Curr Biol 23:70–75. https://doi.org/10.1016/j.cub.2012.11.031.
42. Patwari P, Chutkow WA, Cummings K, Verstraeten VL, Lammerding J, Schreiter ER, Lee RT. 2009. Thioredoxin-independent regulation of metabolism by the alpha-arrestin proteins. J Biol Chem 284:24996–25003. https://doi.org/10.1074/jbc.M109.018093.
43. Tenson T, Ehrenberg M. 2002. Regulatory nascent peptides in the ribosomal tunnel. Cell 108:591–594. https://doi.org/10.1016/S0092-8674(02)00669-4.
44. Nakatogawa H, Ito K. 2002. The ribosomal exit tunnel functions as a discriminating gate. Cell 108:629–636. https://doi.org/10.1016/S0092-8674(02)00649-9.
45. Onouchi H, Nagami Y, Haraguchi Y, Nakamoto M, Nishimura Y, Sakurai R, Nagao N, Kawasaki D, Kadokura Y, Naito S. 2005. Nascent peptide-mediated translation elongation arrest coupled with mRNA degradation in the CGS1 gene of Arabidopsis. Genes Dev 19:1799–1810. https://doi.org/10.1101/gad.1317105.
46. Onouchi H, Haraguchi Y, Nakamoto M, Kawasaki D, Nagami-Yamashita Y, Murota K, Kezuka-Hosomi A, Chiba Y, Naito S. 2008. Nascent peptide-mediated translation elongation arrest of Arabidopsis thaliana CGS1 mRNA occurs autonomously. Plant Cell Physiol 49:549–556. https://doi.org/10.1093/pcp/pcn028.
47. Law GL, Raney A, Heusner C, Morris DR. 2001. Polyamine regulation of ribosome pausing at the upstream open reading frame of S-adenosylmethionine decarboxylase. J Biol Chem 276:38036–38043.
48. Raney A, Law GL, Mize GJ, Morris DR. 2002. Regulated translation termination at the upstream open reading frame in S-adenosylmethionine decarboxylase mRNA. J Biol Chem 277:5988–5994. https://doi.org/10.1074/jbc.M108375200.
49. Reynolds K, Zimmer AM, Zimmer A. 1996. Regulation of RAR beta 2 mRNA expression: evidence for an inhibitory peptide encoded in the 5′-untranslated region. J Cell Biol 134:827–835. https://doi.org/10.1083/jcb.134.4.827.
50. Parola AL, Kobilka BK. 1994. The peptide product of a 5′ leader cistron in the beta 2 adrenergic receptor mRNA inhibits receptor synthesis. J Biol Chem 269:4497–4505.
51. Keshwani MM, Klammt C, von Daake S, Ma Y, Kornev AP, Choe S, Insel PA, Taylor SS. 2012. Cotranslational cis-phosphorylation of the COOH-terminal tail is a key priming step in the maturation of cAMP-dependent protein kinase. Proc Natl Acad Sci U S A 109:E1221–E129. https://doi.org/10.1073/pnas.1202741109.
52. Dai N, Christiansen J, Nielsen FC, Avruch J. 2013. mTOR complex 2 phosphorylates IMP1 cotranslationally to promote IGF2 production and the proliferation of mouse embryonic fibroblasts. Genes Dev 27:301–312. https://doi.org/10.1101/gad.209130.112.
53. Ladror DT, Frey BL, Scalf M, Levenstein ME, Artymiuk JM, Smith LM. 2014. Methylation of yeast ribosomal protein S2 is elevated during stationary phase growth conditions. Biochem Biophys Res Commun 445:535–541. https://doi.org/10.1016/j.bbrc.2014.01.040.
54. Sauert M, Temmel H, Moll I. 2015. Heterogeneity of the translational machinery: Variations on a common theme. Biochimie 114:39–47. https://doi.org/10.1016/j.biochi.2014.12.011.
55. Billin AN, Eilers AL, Queva C, Ayer DE. 1999. Mlx, a novel Max-like BHLHZip protein that interacts with the Max network of transcription factors. J Biol Chem 274:36344–36350. https://doi.org/10.1074/jbc.274.51.36344.
56. Bild AH, Yao G, Chang JT, Wang Q, Potti A, Chasse D, Joshi MB, Harpole D, Lancaster JM, Berchuck A, Olson JA, Jr, Marks JR, Dressman HK, West M, Nevins JR. 2006. Oncogenic pathway signatures in human cancers as a guide to targeted therapies. Nature 439:353–357. https://doi.org/10.1038/nature04296.
57. Pereira B, Chin SF, Rueda OM, Vollan HK, Provenzano E, Bardwell HA, Pugh M, Jones L, Russell R, Sammut SJ, Tsui DW, Liu B, Dawson SJ, Abraham J, Northen H, Peden JF, Mukherjee A, Turashvili G, Green AR, McKinney S, Oloumi A, Shah S, Rosenfeld N, Murphy L, Bentley DR, Ellis IO, Purushotham A, Pinder SE, Borresen-Dale AL, Earl HM, Pharoah PD, Ross MT, Aparicio S, Caldas C. 2016. The somatic mutation profiles of 2,433 breast cancers refines their genomic and transcriptomic landscapes. Nat Commun 7:11479. https://doi.org/10.1038/ncomms11479.
58. Cancer Genome Atlas Research Network. 2014. Comprehensive molecular profiling of lung adenocarcinoma. Nature 511:543–550. https://doi.org/10.1038/nature13385.
59. Cerami E, Gao J, Dogrusoz U, Gross BE, Sumer SO, Aksoy BA, Jacobsen A, Byrne CJ, Heuer ML, Larsson E, Antipin Y, Reva B, Goldberg AP, Sander C, Schultz N. 2012. The cBio cancer genomics portal: an open platform for exploring multidimensional cancer genomics data. Cancer Discov 2:401–404. https://doi.org/10.1158/2159-8290.CD-12-0095.
60. Gao J, Aksoy BA, Dogrusoz U, Dresdner G, Gross B, Sumer SO, Sun Y, Jacobsen A, Sinha R, Larsson E, Cerami E, Sander C, Schultz N. 2013. Integrative analysis of complex cancer genomics and clinical profiles using the cBioPortal. Sci Signal 6:pl1. https://doi.org/10.1126/scisignal.2004088.
61. Ingolia NT, Brar GA, Rouskin S, McGeachy AM, Weissman JS. 2012. The ribosome profiling strategy for monitoring translation in vivo by deep sequencing of ribosome-protected mRNA fragments. Nat Protoc 7:1534–1550. https://doi.org/10.1038/nprot.2012.086.